Communication

Not peer-reviewed version

Development and Characterization of Human Oligodendroglioma Cellular Model as a Useful Tool to Study Iron Role in Tumor Cell: Preliminary Results and Future Prospective

Stefania Braidotti , Debora Curci , Daniele Zampieri , Cesare Covino , Davide Zanon , Natalia Maximova * , Roberto Sala

Posted Date: 15 September 2023

doi: 10.20944/preprints202309.1053.v1

Keywords: Oligodendroglioma; iron; pediatric; brain tumors

Communication

Development and Characterization of Human Oligodendroglioma Cellular Model as a Useful Tool to Study Iron Role in Tumor Cell: Preliminary Results and Future Prospective

Stefania Braidotti [1], Debora Curci [2], Daniele Zampieri [3], Cesare Covino [4], Davide Zanon [5], Natalia Maximova [1,*] and Roberto Sala [6]

[1] Department of Pediatrics, Institute for Maternal and Child Health-IRCCS Burlo Garofolo, Trieste; stefania.braidotti@burlo.trieste.it; natalia.maximova@burlo.trieste.it
[2] Advanced Translational Diagnostic Laboratory, Institute for Maternal and Child Health-IRCCS Burlo Garofolo, Trieste; debora.curci@burlo.trieste.it
[3] Department of Chemical and Pharmaceutical Sciences, University of Trieste, Trieste, Italy; dzampieri@units.it
[4] Advanced Light and Electron Microscopy Imaging Centre (ALEMBIC), IRCCS San Raffaele Scientific Institute, Milan, Italy; covino.cesare@hsr.it
[5] Pharmacy and Clinical Pharmacology Department, Institute for Maternal and Child Health-IRCCS Burlo Garofolo, Trieste, Italy; davide.zanon@burlo.trieste.it
[6] Department of Medicine and Surgery, University of Parma, Parma, Italy; roberto.sala@unipr.it
* Correspondence: natalia.maximova@burlo.trieste.it (N.M.)

Abstract: Oligodendroglioma (OG) is a brain tumor that contributes to < 1% of brain tumor diagnoses in the pediatric population. Unfortunately, pediatric OG remains without definitive molecular characteristics to aid in diagnosis, and little is known about the tumor microenvironment. Tumor cells' metabolism and proliferation rate are generally higher than healthy cells, so their iron demand is also significantly increased. This consideration underlines the great importance of iron for tumor development and progression. In this context, this study aims to evaluate the effect of iron in a cellular in vitro model of human oligodendroglioma brain tumor. Cell morphology, the effect of siderotic medium on cell growth, iron uptake, and the expression of iron metabolism-related genes were evaluated by optic microscopy, ICP-MS, confocal microscopy and RealTime PCR, respectively. This study underlines the great importance of iron for tumor development and progression, but also the possibility of reducing the available iron concentration to determine an antiproliferative effect on OGs. Therefore, every attempt can be promising to defeat the OGs for which there are currently no long-term curative therapies.

Keywords: oligodendroglioma; iron; pediatric; brain tumors

1. Introduction

Brain tumors are the first common tumor and the first cause of tumor death in children, accounting for 25% of childhood cancers and second only to leukemia in frequency [1,2]. Brain tumors can be classified based on origin, glial or not, and represent a dramatic health problem due to their high morbidity and mortality in all ages [3].

Oligodendroglioma (OG, ORPHA:251627, OMIM: 137800, 616568) is a rare subtype of glioma originating from oligodendrocytes, with a limited response to the current standard of treatment [4]. It contributes to < 1% of brain tumor diagnoses in the pediatric population, where it is much less prevalent than in adults. Knowledge about pediatric OG is not well explored, with few studies examining different treatment approaches and outcomes [4]. The overall 5-year survival for grade II

 doi:10.20944/preprints202309.1053.v1

OG in the pediatric population is estimated to be 90%, while for grade III anaplastic OG, it is only 53% [5]. The standard of care for pediatric OG includes surgical resection, radiation, and a regimen of chemotherapy [6].

Given their rarity, the literature is sparse. Current knowledge states that pediatric OGs are often molecularly distinct from their adult counterparts and often lack the 1p/19q co-deletion or IDH mutation. However, little is known about the pediatric tumor microenvironment.

Tumor cells' metabolism and proliferation rate are generally higher than healthy cells, so their iron demand is also significantly increased. Several epidemiological studies have investigated the association between body iron levels and cancer, supporting a positive association in adults [7]. The central nervous system is not directly in contact with the plasma iron pool because it resides behind the blood-brain barrier (BBB). Like many molecules, the entry of iron is tightly regulated by the BBB, and specific transport mechanisms are required to transfer iron into the brain tissue [8,9].

Pieces of evidence have shown that iron metabolism is closely related to glial cell tumorigenesis, tumor progression, and tumor resistance microenvironment, although key iron metabolism-related genes are unclear [8,10,11]. Since tumor cells strongly depend on iron for their growth/proliferation, they are more sensitive to iron depletion than normal cells [12]. It is unclear whether tumor resistance to conventional therapies occurs because of increased permeability of the BBB due to conventional pharmacological therapies or radiotherapy, allowing massive entry of iron without control. This imbalance in cancer mainly manifests as increased iron metabolism, iron affinity, iron input, and inhibition of its output, resulting in iron accumulation. Elevated serum ferritin levels are observed in several types of cancer; however, little is known about the association between ferritin and glioma [13]. Only a few studies have assessed the ferritin levels in gliomas by routine laboratory diagnostics. However, the biological background of glioma-associated ferritinemia remains not well elucidated.

This consideration underlines the great importance of iron for tumor development and progression, but also the possibility of reducing the available iron concentration to determine an antiproliferative effect on OG. This study is part of a larger research project that aims to study iron permeability across the blood-brain barrier as a trigger for the onset of brain tumors in pediatric patients with long-term survival after acute lymphoblastic leukemia treatments [14-16]. In this work, we focused on establishing an *in vitro* model of human oligodendroglioma brain tumors and to characterize cells undergoing siderotic culture conditions.

2. Materials and Methods

2.1. Cell Lines and Culture Conditions

The study was performed on immortalized human oligodendroglioma cell line (HOG) purchased from Sigma-Aldrich (SCC163, Merck KGaA, Germany) [17,18]. We develop a siderotic HOG cell line model by culturing HOG cells for three months in Low glucose Dulbecco's modified Eagle's medium (LG-DMEM) (ECM0749, EuroClone SpA, Italy) in which the concentration of ferric nitrate is 0.25 μM), supplemented with 1 % fetal bovine serum (10270106 FBS, Origin Brazil, Gibco-Thermo Fisher Scientific, Italy) 2 mM glutamine (35050,GlutaMAX Gibco- Thermo Fisher Scientific, Italy) and 1% Penicillin-Streptomycin solution (A8943,AppliChem) enriched with 100 μM of ferric citrate (F3388, Merck KGaA, Germany). We cultured HOG cells, our control cells, in complete culture medium, without any ferric citrate supplement (the complete medium's iron concentration did not exceed 0.75 μM). Cells were kept in cell culture flasks (#833911.002 Sarstedt, Nümbrecht, Germany) at 37°C in a humidified atmosphere with 5% CO_2. Cell culture experiments were conducted at Parma University.

2.2. Viability measurements (AlamarBlue assay)

To analyze the cells' growth kinetic, cells were plated in 96-well plates (#833924 Sarstedt, Nümbrecht, Germany) (5,000 cells/well for both siderotic and control cells) and then incubated in complete culture medium supplemented or not with 10 μM of ferric citrate. After the indicated time, the growth medium was replaced with 120 μl of resazurin solution in DMEM (10 μg/ml) for one hour

 doi:10.20944/preprints202309.1053.v1

at 37°C. Relative fluorescent units (RFU) emitted by resorufin were acquired from 100µL samples by EnSpire® Multimode Plate Reader (Perkin Elmer, Waltham, MA, USA) λ ex/ λ em. 540/ 585nm).

Quadrupled wells were measured for each time point. The experimental setting was repeated at least three times. Cell growth kinetic was performed starting from day 0; analyses at days +1, + 2, +4, +7, +9, +11, +14, +16, +18, +21, and +23 were considered.

2.3. Sample preparation for ICP-MS analysis in cell lines

Control and siderotic HOG cells were seeded onto 24 well plates (#833922-Sarstedt, Nümbrecht, Germany) at a density of 40,000 cells/cm². The day after, the medium was substituted with a growth medium either based on DMEM supplemented or not with 25 µM or 100 µM of ferric citrate. After the incubation, cells were washed 5 times with PBS and detached by trypsin solution. After trypsin neutralization with DMEM + 10% FBS, the cell suspension was centrifuged for 5 min at 200 xg, thereafter the pellets were fixed in 100 µl of paraformaldehyde solution, 4% in PBS, for 10 min at 4°C.

2.4. Quantification of iron (Fe) in cell lysates

Quantification of iron (Fe) in cell lysates. Samples were added 50 µL of nitric acid 69% (VWR International S.r.l., Milan, Italy) and diluted to a final volume of 5 mL with Milli-Q water (Millipore purification pack system, Millipore, Massachusetts, USA). Cell samples were mineralized with 200 µL of nitric acid, 69%, and 50 µL of Hydrogen Peroxide 30% (Sigma-Aldrich, Italy). Subsequently, cells were sonicated for 15 minutes and diluted to 5 mL with Milli-Q water.

ICP-MS Nexion 350X with an ESI autosampler (Perkin Elmer, Waltham, Massachusetts, MA, USA) was used to determine the total Fe concentrations in cell lysates derived from the mineralization. Five-point standard curves obtained by dilution of Fe standard solutions (10000 µg/L) for ICP analysis (Sigma-Aldrich) were used for ICP-MS measurements (range 0.01–100 µg/L; ion mass: 54 and 57 u.m.a. for Fe). Laboratory-fortified blanks and laboratory-fortified samples (1 µg/L and 10 µg/L) analyzed before and after the sample solutions were used to assess the matrix effects.

The recovery for Fe was always > 95%. The limit of detection was 0.1 µg/L for Fe, and the precision of the measurements as repeatability (relative standard deviation (RSD) %) for the analysis was < 3%.

2.5. Confocal Laser Scanning Microscope analysis

Confocal fluorescence microscopy was accomplished at the Confocal Microscopy Laboratory DIMEC- University of Parma.

Cells were seeded into 35 mm cell view culture dishes, with glass bottom (627860 Greiner Bio-One S.r.l., Italy) in complete medium supplemented or not with ferric citrate. Before the analysis, cells were rinsed twice in PBS and incubated for one hour in a complete medium supplemented or not with 10 µM of ferric citrate, in the presence of 5 µM Rhonox-1, and 1.6 µM LysoTracker® Yellow HCK-123. For nuclei counterstaining, 5 µg/mL of Hoechst 33-258 was added to all the tested conditions during the last 20 minutes of incubation.

Dishes were inserted into a heated chamber (Oko UNO Stage Inc Set Premix Inv K-Frame. 158006102- Okolab https://okolab4microsystems.com/) warmed to 37°C with 5% CO2. All images were collected with a Leica TCS SP5 Laser Scanning Confocal microscope (Leica Microsystems, Wetzlar, Germany), equipped with a 405 nm (Diode) laser line (LL) and an HCX PL APO λ blue 63X (NA 1.4) Oil objective, and LAS X 4.3.0.24308 microscope software. Single confocal sections adopted independent configuration settings to avoid any possible crosstalk during acquisition. The emission of Rhonox-1 signal excited at 540 nm LL was collected with a spectral detection ranging from 548 to 647 nm. Hoechst 33-258 was excited at 405nm LL (laser line) with a spectral detection ranging from 420nm to 486nm.

The co-localization of Fe2+ and lysosomes was evaluated using the following setting: Hoechst 33-258 was excited at 405 nm LL (laser line) with a spectral detection ranging from 410nm to 459 nm. LysoTracker® Yellow HCK-123 was excited at 485 nm, and emission was collected with a spectral

Preprints (www.preprints.org) | NOT PEER-REVIEWED | Posted: 15 September 2023 doi:10.20944/preprints202309.1053.v1

detection ranging from 571 to 705 nm. Rhonox-1 probe was excited at 543nm LL (Laser Line), and emission was collected with a spectral detection ranging from 552 nm to 599 nm. Fluorescence intensity of the single cells was acquired and images were analyzed with ImageJ software. Thereafter, we calculated the Corrected Total Cell Fluorescence (CTCF) for each cell with the following formula:

CTCF = Integrated Density – (Area of selected cell X Mean fluorescence of background readings). Data of intracellular Fe^{2+} was expressed in each cell as CTCF/ area of the selected cell. CTCF was measured in 69 cells of the control group (HOG LG-DMEM), 73 cells of HOG LG DMEM+ 10 μM Fe-citrate, and 57 cells of HOG100 LG-DMEM + 10 μM of Fe-citrate population.

Additional analyses were carried out in ALEMBIC, an advanced microscopy laboratory established by IRCCS Ospedale San Raffaele and Università Vita-Salute San Raffaele (Supplementary Material).

2.6. Gene expression by Real-time PCR analysis

Total RNA was extracted from HOG, HOG 100 μM cultured with iron citrate, and HOG 100 μM cultured without iron citrate, using the Monach® Total RNA Miniprep Kit (#T2010S, New England BioLabs. Inc, USA) according to the manufacturer's instructions, and quantified using Nanodrop 2000 spectrophotometer (ThermoFisher Scientific, Italy). One μg RNA/sample was reversed-transcribed into cDNA using the RevertAid RT Reverse Transcription Kit (#00771469, ThermoFisher Scientific, Italy).

The analysis of gene expression was performed by real-time PCR using Luna® Universal qPCR Master Mix (#M3003E, New England Biolabs Inc., USA) along with the forward and reverse primers (5 pmol each) reported in Table 1. The primer sets were designed according to the known sequences reported in GenBank with Primer 3 program [19] (Code available at http://www-genome.wi.mit.edu/genome_software/other/primer3.html). Real-time PCR was performed in a RotorGene 3000 apparatus (Corbett). A melting curve analysis was added at the end of each amplification cycle.

Table 1. Primer sequences (from https://primer3.ut.ee/) for real-time PCR analysis.

Gene name	Gene bank number	Primer Sequence (5′-3′)	Product size (bp)	Annealing temperature (°C)	Primer efficency
GAPDH	NM_002046	Forward TCTCTGCTCCTCCTGTTC Reverse GCCCAATACGACCAAATCC	120	60	1.08
FTH1	NM_002032	Forward ACCTGTCCATGTCTTACTACTTTG Reverse GCCACCTCGTTGGTTCTG	134	60	1.03
FTL	NM_000146	Forward GCCTCCTACACCTACCTCTC Reverse GCTGGCTTCTTGATGTCCTGG	179	60	1.16
MYC	NM_002467.4	Forward GCGACTCTGAGGAGGAACA Reverse TGCGTAGTTGTGCTGATGTG	182	59	0.96
RPL15	NM_002948	Forward GGAGAAAGAAGCAGTCTGATGTC Reverse CCACGGCGAACACGAATC	175	60	1.06
TUBB3	NM_006086	Forward GCAAGGTGCGTGAGGAGTAT Reverse GCGGAAGCAGATGTCGTAGA	182	60	1.00

The data analysis was conducted according to the Pfaffl formula [20], and *RPL15* was used as housekeeping.

$$Ratio = \frac{Etag^{\Delta CTtag\,(control-sample)}}{Eref^{\Delta CTref\,(control-sample)}} \quad (1)$$

 doi:10.20944/preprints202309.1053.v1

2.8. Statistical analysis

Graphical representation and statistical analysis were performed using the GraphPad Prism 8.0 software (La Jolla, CA; USA).

Growth curve data were best fitted with the Gompertz growth model and analyzed by the extra sum-of-squares F test. Data are shown as mean ±SD. Asterisks indicate statistical significance (* $p<0.05$; ** $p<0.01$; *** $p<0.001$).

Statistical differences in the intracellular iron quantity, and of real-time PCR data, among groups were determined using 2way ANOVA, followed by Sidak's multiple comparisons test. CTCF/area data were analyzed with 1way ANOVA followed by Tukey's multiple comparisons test.

Differences were considered significant when $p < 0.05$.

3. Results

3.1. Effect of iron conditioning on cell morphology

By visual microscope analysis (Figure 1), HOG cells show an epithelioid-like and oligodendrocyte-like morphology; cells appear flat with long and thin extensions and a high nucleus/cytoplasm ratio.

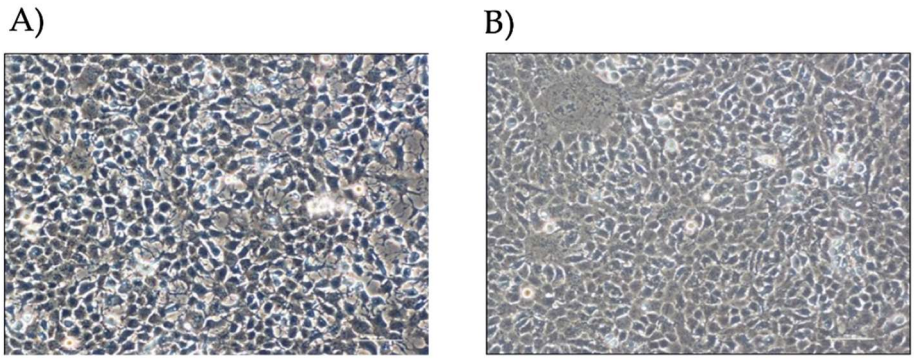

Figure 1. HOG cells by optical microscope. A) HOG LG-DMEM, 1% FBS; B) HOG LG-DMEM,1% FBS ,100 μM Fe-citrate.

3.2. Effect of medium composition on cell models

The iron content was evaluated in cells cultured in their medium and in cells that changed medium for 24 hours.

Intracellular iron, measured with ICP-MS was significantly different between cells grown in 100 μM of ferric citrate compared to non-conditioned HOG cells (2439 ± 722.3 fg/cell vs 31.72 ± 7.59 fg/cell, $p<0.001$) even in medium without ferric citrate solution (Figure 2).

Preprints (www.preprints.org) | NOT PEER-REVIEWED | Posted: 15 September 2023 doi:10.20944/preprints202309.1053.v1

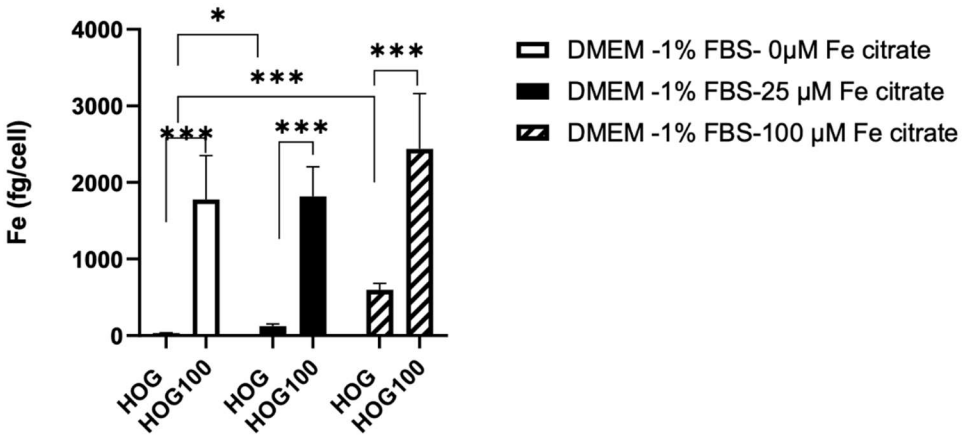

Figure 2. Effects of 24-hour incubation of medium with different iron concentrations on the intracellular iron content of HOG cells.

Interestingly, a 24-hour medium switch induced variation in intracellular iron in both cell types. Intracellular iron decreased in HOG100 switched for 24 hours in medium without ferric citrate (1776.91 ± 576.17 fg/cell) but increased in control HOG cells switched for 24 hours to 25 μM (122.51 ± 29.86, $p<0.01$) or 100 μM ferric citrate-LG-DMEM (597.6 ± 83.8 fg/cell, $p<0.001$).

3.3. Cell line viability and proliferation after conditioned iron medium

We monitored the iron-conditioned cells' behavior (HOG 100 μM) regarding proliferation and growth in two different culture conditions (with and without ferric citrate 10 μM), versus non-conditioned HOG cells.

The growth curves generated by the Gompertz model reflect a classic growth curve pattern and were not different between siderotic (HOG100) and control cells either grown in LG-DMEM- 1% FBS with or without 10 μM of ferric citrate, a concentration ten folds higher of the CSF iron detected in transfused patients (HOG100 vs HOG; $p=0.3044$) but lower than the serum levels (48.92 ± 12.97 μM).

Cell viability significantly changed when cells were switched from LG-DMEM to LG-DMEM plus 10 μM ferric citrate, showing an enhancement in medium enriched with ferric citrate ($p<0.0001$, Figure 3). Specifically, the exponential phase of both HOG and HOG 100 μM cultured in media supplemented with ferric citrate 10 μM, lasts longer than the condition without medium supplementation (YM= 70348 vs 190618, $p<0.0001$), and the lag phase was shorter (K= 0.048 vs 0.017; $p<0.05$).

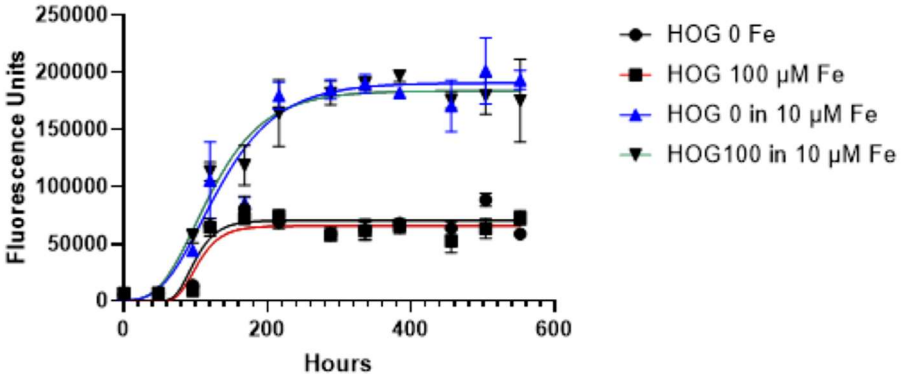

Preprints (www.preprints.org) | NOT PEER-REVIEWED | Posted: 15 September 2023 doi:10.20944/preprints202309.1053.v1

Figure 3. Growth curve of HOG and HOG 100μM cell lines. Cells were cultured in a standard culture medium in the presence or absence of ferric citrate 10 μM. Cell viability was evaluated by resazurin metabolic conversion into living cells. Least squares regression was used and data were best fitted by the Gompertz growth model. Data are expressed as mean ± standard error (SE) from at least three independent experiments for each cell line. Analysis was performed with GraphPad software. (H. J. Motulsky, GraphPad Curve Fit-ting Guide). http://www.graphpad.com/guides/prism/7/curve-fitting/index.htm.

3.4. Confocal microscopy confirms the iron uptake

When HOGs were incubated with RhoNox-1 an active fluorescent probe that specifically detects unstable Fe^{2+}, the increment of the Fe^{2+} molecules inside the cells incubated with high iron-containing media, was observable mainly in mitochondria and cytoplasm (Figure 4 and Figure S1). We observed a significative increment of RhoNox-1 fluorescence after 24 hours of switching to 10 μM Fe citrate LG-DMEM. The analysis of co-localization with ImageJ [21] showed that only 1% of the Fe^{2+} was localized in the lysosomal compartment. Some of the RhoNox-1 fluorescence was also detected in the nuclei, suggesting a possible role of Fe^{2+} in the regulation of gene expression.

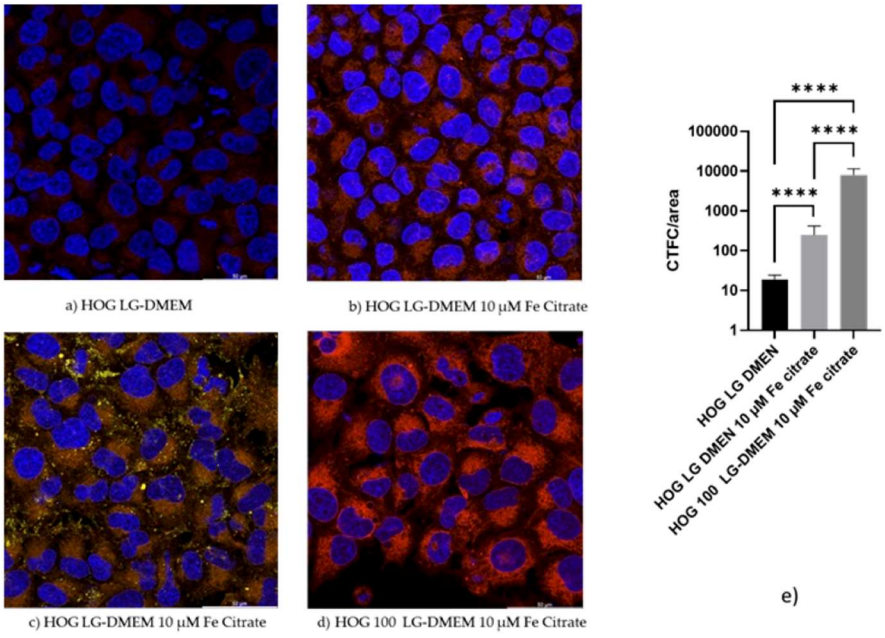

Figure 4. Confocal images of HOG and HOG100 cells. Cells were cultured in a standard culture medium in the presence or absence of ferric citrate 10 μM for 24 hours. Thereafter, cells were incubated for one hour in a complete medium supplemented or not with 10 μM of ferric citrate, in the presence of 5 μM Rhonox-1 (red) and 1.6 μM LysoTracker® Yellow HCK-123 (yellow). For nuclei counterstaining, 5 μg/mL of Hoechst 33-258 (blue) was added to all the tested conditions during the last 20 min. of incubation. Images collected with a Leica TCS SP5 Laser Scanning Confocal microscope (Leica Microsystems, Wetzlar, Germany).

3.5. Gene expression

To investigate the results shown by the Alamar-blue assay, we investigate the effects on the expression of representative genes related to cell growth and iron metabolism, in HOG cells (Figure 5).

Preprints (www.preprints.org) | NOT PEER-REVIEWED | Posted: 15 September 2023 doi:10.20944/preprints202309.1053.v1

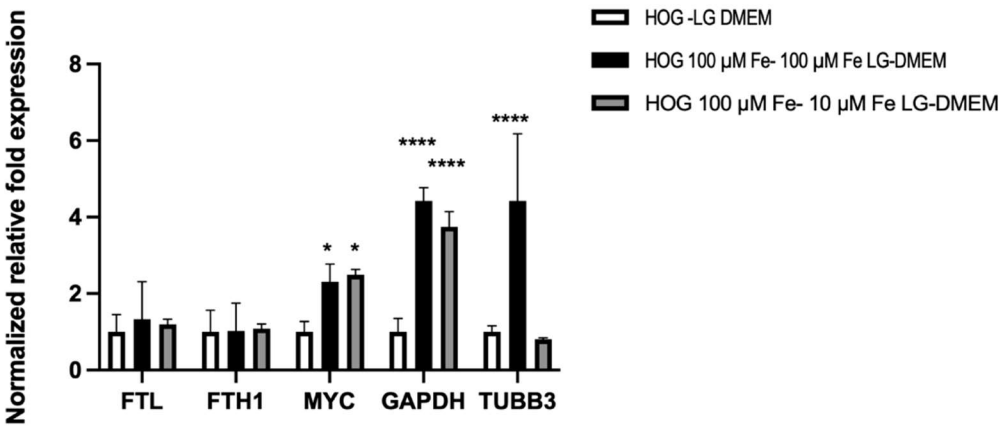

Figure 5. Gene expression analysis of HOG and HOG100 in LG DMEM + 10 µM Fe-citrate for 24 hours.

The expression of heavy and light chains of ferritin (*FTH1*, *FTL*), that organize the cell iron storage system, didn't change among all the tested conditions. On the contrary, *c-MYC* was significantly induced by media with elevated iron concentrations (100 µM Fe-citrate LG-DMEM 2.31 ± 0.45 folds; 10µM Fe-citrate LG-DMEM 2.49 ± 0.14 folds). The gene coding for the moonlighting protein glyceraldehyde 3-phosphate (*GAPDH*) was strongly induced by iron-enriched media (100 µM Fe-citrate LG-DMEM 4.42±0.35 folds; 10µM Fe-citrate LG DMEM 3.74±0.45 folds) and the 24 hours switch from 100 µM Fe citrate to 10 µM Fe-citrate LG-DMEM didn't affect its expression. Tubulin Beta 3 (*TUBB3*) expression was highly induced in 100 µM Fe-citrate enriched medium (4.42 ± 1.77 folds vs LG-DMEM) but was normalized in 24 hours, when switched to 10 µM Fe-citrate medium (0.8 ± 0.046 folds).

4. Discussion

Previous studies have shown that HOG cells have a duplication time of about 18 hours and a rather heterogeneous phenotype: they express some oligodendrocyte-specific proteins, including A2B5, a 15 kDa form of the basic protein of the myelin (MBP) and cyclic 2',3'-nucleotide3'-phosphodiesterase (CNPase); even the lysosomal protein galactosylceramide (GalC), sulfogalactosylceramide, vimentin, and cytokeratin K7 were found to be expressed [17,22,23]. Data collected from Buntinx et al. show that HOG is a model of human oligodendrocytes 'arrested' in an immature developmental stage. Culturing in the appropriate medium can induce further differentiation of these cells [18].

Thanks to cell viability assays, it was possible to evaluate how HOG and HOG 100 µM growth can be influenced by the presence of iron in the cell culture medium. Generally, the classical growth curve pattern includes a lag phase after culture seeding, followed by a log phase in which cells proliferate and grow exponentially.

Finally, the stationary phase occurs when the growth medium is spent or when the cells occupy all the available substrates. The main difference in terms of growth is observed by comparing the presence or absence of iron in the medium, regardless of the preconditioning of the cells with iron. The exponential phase of both HOG and HOG 100 µM lasts longer in time, reaching the stationary phase almost at the end of the experiment after two weeks of cell culture. We can hypothesize that the different conditions offered by the addition of the 10 µM ferric citrate solution may favor a more advantageous growth and proliferation condition in tumoral cells as well as in healthy oligodendrocytes. It is known that because of their elevated metabolic needs associated with myelination, oligodendrocytes have the highest iron levels in the brain [24]. Brown and colleagues have observed an increased intercellular iron import in cancer cells [25]. It is known that iron

promotes cell growth and proliferation, but it also causes oxidative stress damage. In particular, the aberrant accumulation of iron and subsequent excess ROS cause oxidative stress, which leads to genome and epigenome alterations giving rise to tumor heterogeneity and evolving metastatic potential [25].

During viability assays, cells were also observed at the microscope and were viable, proliferating, and characterized by an oligodendrocyte-like morphology appearing flat with long and thin extensions and a high nucleus/cytoplasm ratio. Human oligodendroglial cell line HOG presents oligodendrocyte-associated features [17,18].

Confocal observations showed that Rhonox-1 signal, linked to Fe^{2+}, is mainly compartmentalized. It is strongly increased after a 24-hour incubation in a medium containing 10 μM of Fe, a concentration detected in the serum of patients with systemic siderosis. Most of the signal is in mitochondria and vesicles. Fe^{2+} is a form of iron that through the Fantom reaction induces the production of free radicals leading to lipid peroxidation and ferroptosis. During our observation, we did not detect any sign of apoptosis meaning that at least in HOG cells, the excess of Fe^{2+} is neutralized by mechanisms that require further investigation. Although 100 μM of extracellular iron is a condition that is never detected in vivo, our data support the importance of extracellular iron in the behavior of tumor cells. It is well known that cancer cells could release small extracellular vesicles that allow the transport of substances, among which iron, from the cells themselves to communicate with their environment [26]. The removal of intracellular iron by vesicles is an important mechanism driving ferroptosis and so tumor progression.

The HOG cell lines all exhibited markers of immature oligodendrocytes. Growing evidence suggests that iron-associated proteins, such as ferritin and the proto-oncogene c-MYC, contribute to the growth of malignant tumor cells. Ali and colleagues demonstrated that *FTH1* silencing promoted cell growth in breast cancer leading to an increased c-MYC expression, and reduced cell sensitivity to chemotherapy [27,28]. Our data documented no change in *FTH1* and *FTL* gene expression, but *c-MYC* was significantly induced by media with elevated iron concentrations, supporting the higher proliferation rate observed in the HOG cell line.

We also observed a strong induction of *GAPDH* expression. Previous studies have revealed that GAPDH acts as a receptor for iron carrier proteins [29]. Iron is increasingly linked to cancer, such as neuroblastoma because there is an elevated requirement for iron that favors cancer progression. However, it is unclear whether GAPDH-mediated iron uptake has any role in ferroptosis: cancer cells might utilize iron to favor their progression and to increase their invasive capability [29]. GAPDH localizes not only in the cytosol, but this protein is detected also in the membrane, the nucleus, polysomes, the ER, and the Golgi. GAPDH has been shown to regulate microtubule assembling and vesicular trafficking from ER to Golgi apparatus being involved in the early secretory pathway [30].

Our data show that iron-rich media prompt the expression of *TUBB3*; probably iron lead to increased message stability favoring gene transcription. *TUBB3* is frequently overexpressed in human tumors and is associated with resistance to microtubule-targeting agents, tumor aggressiveness, and poor patient outcomes. Together with tubulin, GAPDH could be part of a cellular response to the increased iron uptake which is remodeled by the reduction of the iron in the microenvironment.

5. Conclusions

In conclusion, this work provides new insight into the great importance of iron for tumor development and progression. An innovative therapeutic approach that includes iron concentration reduction in tumor cells could be used to determine an antiproliferative effect permitting the achievement of better clinical outcomes in pediatric patients suffering from OG.

Supplementary Materials: The following supporting information can be downloaded at the website of this paper posted on Preprints.org. Figure S1: Confocal images of HOG100 cells in 10 μM of ferric citrate.; Table S1: Effects of 24-hour incubation of medium with different iron concentrations on the intracellular iron content of HOG cells.

Author Contributions: Conceptualization, R.S. and N.M.; methodology, R.S., N.M., C.C., D.Z.; validation, R.S., N.M., C.C., D.Z.; formal analysis, S.B., D.C., N.M., R.S.; investigation, R.S., N.M., C.C, D.Z.; resources, R.S., N.M., C.C, D.Z.; data curation, R.S., C.C., D.Z.; writing—original draft preparation, S.B., D.C., R.S., N.M.; writing—review and editing, S.B., D.C. R.S., N.M.; visualization, S.B., D.C. R.S., N.M.; supervision, R.S. and N.M.; project administration, R.S. and N.M.; funding acquisition, R.S. and N.M. All authors have read and agreed to the published version of the manuscript.

Funding: This work was supported by the Italian Ministry of Health, through the contribution given to the Institute for Maternal and Child Health IRCCS Burlo Garofolo, Trieste, Italy.

Institutional Review Board Statement: The study did not require ethical approval.

Informed Consent Statement: Not applicable.

Data Availability Statement: The original contributions presented in this communication are included in the article. Further inquiries can be directed to the corresponding author.

Acknowledgments: Part of this work was carried out in ALEMBIC, an advanced microscopy laboratory established by IRCCS Ospedale San Raffaele and Università Vita-Salute San Raffaele and in Laboratorio di Microscopia Confocale DIMEC- Università degli studi di Parma.

Conflicts of Interest: The authors declare no conflict of interest.

References

1. Singla, A.K.; Madan, R.; Gupta, K.; Goyal, S.; Kumar, N.; Sahoo, S.K.; Uppal, D.K.; Ahuja, C.K. Clinical behaviour and outcome in pediatric glioblastoma: current scenario. *Radiation oncology journal* **2021**, *39*, 72-77, doi:10.3857/roj.2020.00591.
2. Ostrom, Q.T.; Adel Fahmideh, M.; Cote, D.J.; Muskens, I.S.; Schraw, J.M.; Scheurer, M.E.; Bondy, M.L. Risk factors for childhood and adult primary brain tumors. *Neuro-oncology* **2019**, *21*, 1357-1375, doi:10.1093/neuonc/noz123.
3. Li, S.; Wang, C.; Chen, J.; Lan, Y.; Zhang, W.; Kang, Z.; Zheng, Y.; Zhang, R.; Yu, J.; Li, W. Signaling pathways in brain tumors and therapeutic interventions. *Signal Transduction and Targeted Therapy* **2023**, *8*, 8, doi:10.1038/s41392-022-01260-z.
4. Lau, C.S.; Mahendraraj, K.; Chamberlain, R.S. Oligodendrogliomas in pediatric and adult patients: an outcome-based study from the Surveillance, Epidemiology, and End Result database. *Cancer management and research* **2017**, *9*, 159-166, doi:10.2147/CMAR.S117799.
5. Byer, L.; Kline-Nunnally, C.; Tihan, T.; Mueller, S. Chapter 33 - Pediatric oligodendroglioma. In *Oligodendroglioma*, Paleologos, N.A., Newton, H.B., Eds.; Academic Press: 2019; pp. 379-386.
6. Goel, N.J.; Abdullah, K.G.; Lang, S.-S. Outcomes and Prognostic Factors in Pediatric Oligodendroglioma: A Population-Based Study. *Pediatric Neurosurgery* **2017**, *53*, 24-35, doi:10.1159/000481458.
7. Fonseca-Nunes, A.; Jakszyn, P.; Agudo, A. Iron and Cancer Risk—A Systematic Review and Meta-analysis of the Epidemiological Evidence. *Cancer Epidemiology, Biomarkers & Prevention* **2014**, *23*, 12-31, doi:10.1158/1055-9965.EPI-13-0733.
8. Hänninen, M.M.; Haapasalo, J.; Haapasalo, H.; Fleming, R.E.; Britton, R.S.; Bacon, B.R.; Parkkila, S. Expression of iron-related genes in human brain and brain tumors. *BMC neuroscience* **2009**, *10*, 36-36, doi:10.1186/1471-2202-10-36.
9. Liu, H.-D.; Li, W.; Chen, Z.-R.; Zhou, M.-L.; Zhuang, Z.; Zhang, D.-D.; Zhu, L.; Hang, C.-H. Increased expression of ferritin in cerebral cortex after human traumatic brain injury. *Neurological Sciences* **2013**, *34*, 1173-1180, doi:10.1007/s10072-012-1214-7.
10. Legendre, C.; Garcion, E. Iron metabolism: a double-edged sword in the resistance of glioblastoma to therapies. *Trends in Endocrinology & Metabolism* **2015**, *26*, 322-331, doi:10.1016/j.tem.2015.03.008.
11. Reith, T.P.; Prah, M.A.; Choi, E.-J.; Lee, J.; Wujek, R.; Al-Gizawiy, M.; Chitambar, C.R.; Connelly, J.M.; Schmainda, K.M. Basal Ganglia Iron Content Increases with Glioma Severity Using Quantitative Susceptibility Mapping: A Potential Biomarker of Tumor Severity. *Tomography* **2022**, *8*, 789-797, doi:10.3390/tomography8020065.
12. Schonberg, David L.; Miller, Tyler E.; Wu, Q.; Flavahan, William A.; Das, Nupur K.; Hale, James S.; Hubert, Christopher G.; Mack, Stephen C.; Jarrar, Awad M.; Karl, Robert T.; et al. Preferential Iron Trafficking Characterizes Glioblastoma Stem-like Cells. *Cancer Cell* **2015**, *28*, 441-455, doi:10.1016/j.ccell.2015.09.002.
13. Jaksch-Bogensperger, H.; Spiegl-Kreinecker, S.; Arosio, P.; Eckl, P.; Golaszewski, S.; Ebner, Y.; Al-Schameri, R.; Strasser, P.; Weis, S.; Bresgen, N. Ferritin in glioblastoma. *British Journal of Cancer* **2020**, *122*, 1441-1444, doi:10.1038/s41416-020-0808-8.

14. Walter, A.W.; Hancock, M.L.; Pui, C.H.; Hudson, M.M.; Ochs, J.S.; Rivera, G.K.; Pratt, C.B.; Boyett, J.M.; Kun, L.E. Secondary brain tumors in children treated for acute lymphoblastic leukemia at St Jude Children's Research Hospital. *Journal of Clinical Oncology* **1998**, *16*, 3761-3767, doi:10.1200/JCO.1998.16.12.3761.
15. Maule, M.; Scélo, G.; Pastore, G.; Brennan, P.; Hemminki, K.; Tracey, E.; Sankila, R.; Weiderpass, E.; Olsen, J.H.; McBride, M.L.; et al. Risk of Second Malignant Neoplasms After Childhood Leukemia and Lymphoma: An International Study. *JNCI: Journal of the National Cancer Institute* **2007**, *99*, 790-800, doi:10.1093/jnci/djk180.
16. Alexiou, G.A.; Moschovi, M.; Georgoulis, G.; Neroutsou, R.; Stefanaki, K.; Sfakianos, G.; Prodromou, N. Anaplastic oligodendrogliomas after treatment of acute lymphoblastic leukemia in children: Report of 2 cases. *Journal of Neurosurgery: Pediatrics PED* **2010**, *5*, 179-183, doi:10.3171/2009.9.PEDS09154.
17. Post, G.R.; Dawson, G. Characterization of a cell line derived from a human oligodendroglioma. *Molecular and Chemical Neuropathology* **1992**, *16*, 303-317, doi:10.1007/BF03159976.
18. Buntinx, M.; Vanderlocht, J.; Hellings, N.; Vandenabeele, F.; Lambrichts, I.; Raus, J.; Ameloot, M.; Stinissen, P.; Steels, P. Characterization of three human oligodendroglial cell lines as a model to study oligodendrocyte injury: Morphology and oligodendrocyte-specific gene expression. *Journal of Neurocytology* **2003**, *32*, 25-38, doi:10.1023/A:1027324230923.
19. Untergasser, A.; Cutcutache, I.; Koressaar, T.; Ye, J.; Faircloth, B.C.; Remm, M.; Rozen, S.G. Primer3--new capabilities and interfaces. *Nucleic acids research* **2012**, *40*, e115-e115, doi:10.1093/nar/gks596.
20. Pfaffl, M.W. A new mathematical model for relative quantification in real-time RT-PCR. *Nucleic acids research* **2001**, *29*, e45-e45, doi:10.1093/nar/29.9.e45.
21. Bolte, S.; CordeliÈRes, F.P. A guided tour into subcellular colocalization analysis in light microscopy. *Journal of Microscopy* **2006**, *224*, 213-232, doi:10.1111/j.1365-2818.2006.01706.x.
22. Kashima, T.; Tiu, S.N.; Merrill, J.E.; Vinters, H.V.; Dawson, G.; Campagnoni, A.T. Expression of Oligodendrocyte-associated Genes in Cell Lines Derived from Human Gliomas and Neuroblastomas1. *Cancer Research* **1993**, *53*, 170-175.
23. De Kleijn, K.M.A.; Zuure, W.A.; Peijnenborg, J.; Heuvelmans, J.M.; Martens, G.J.M. Reappraisal of Human HOG and MO3.13 Cell Lines as a Model to Study Oligodendrocyte Functioning. *Cells* **2019**, *8*, doi:10.3390/cells8091096.
24. Connor, J.R.; Menzies, S.L. Relationship of iron to oligondendrocytes and myelination. *Glia* **1996**, *17*, 83-93, doi:10.1002/(SICI)1098-1136(199606)17:2<83::AID-GLIA1>3.0.CO;2-7.
25. Brown, R.A.M.; Richardson, K.L.; Kabir, T.D.; Trinder, D.; Ganss, R.; Leedman, P.J. Altered Iron Metabolism and Impact in Cancer Biology, Metastasis, and Immunology. *Frontiers in oncology* **2020**, *10*, 476-476, doi:10.3389/fonc.2020.00476.
26. Alarcón-Veleiro, C.; Mato-Basalo, R.; Lucio-Gallego, S.; Vidal-Pampín, A.; Quindós-Varela, M.; Al-Qatarneh, T.; Berrecoso, G.; Vizoso-Vázquez, Á.; Arufe, M.C.; Fafián-Labora, J. Study of Ferroptosis Transmission by Small Extracellular Vesicles in Epithelial Ovarian Cancer Cells. *Antioxidants (Basel, Switzerland)* **2023**, *12*, 183, doi:10.3390/antiox12010183.
27. Ali, A.; Shafarin, J.; Abu Jabal, R.; Aljabi, N.; Hamad, M.; Sualeh Muhammad, J.; Unnikannan, H.; Hamad, M. Ferritin heavy chain (FTH1) exerts significant antigrowth effects in breast cancer cells by inhibiting the expression of c-MYC. *FEBS Open Bio* **2021**, *11*, 3101-3114, doi:10.1002/2211-5463.13303.
28. Wu, T.; Li, Y.; Liu, B.; Zhang, S.; Wu, L.; Zhu, X.; Chen, Q. Expression of Ferritin Light Chain (FTL) Is Elevated in Glioblastoma, and FTL Silencing Inhibits Glioblastoma Cell Proliferation via the GADD45/JNK Pathway. *PloS one* **2016**, *11*, e0149361-e0149361, doi:10.1371/journal.pone.0149361.
29. Cornett, K.; Puderbaugh, A.; Back, O.; Craven, R. GAPDH in neuroblastoma: Functions in metabolism and survival. *Frontiers in Oncology* **2022**, *12*.
30. Kumagai, H.; Yoshihara, K.; Umemoto, M.; Igarashi, K.; Hirose, S.; Ohgi, K.; Irie, M. Studies on Salivary Gland Ribonucleases. III. Purification and Properties of Three Ribonucleases from Bovine Parotid Gland. *The Journal of Biochemistry* **1983**, *93*, 865-874, doi:10.1093/jb/93.3.865.